Experimental investigation of equivalent Laplacian and adjacency quantum walks on irregular graphs

Dengke Qu,[1,2,*] Lei Xiao,[2] Kunkun Wang,[3] Xiang Zhan,[4,5] and Peng Xue[2,†]

[1]*Department of Physics, Southeast University, Nanjing 211189, China*
[2]*Beijing Computational Science Research Center, Beijing 100084, China*
[3]*School of Physics and Optoelectronics Engineering, Anhui University, Hefei 230601, China*
[4]*School of Science, Nanjing University of Science and Technology, Nanjing 210094, China*
[5]*MIIT Key Laboratory of Semiconductor Microstructure and Quantum Sensing, Nanjing University of Science and Technology, Nanjing 210094, China*

(Received 27 February 2022; accepted 9 June 2022; published 27 June 2022)

The continuous-time quantum walk denotes the evolution of a particle on a given graph governed by Schrödinger's equation. For different applications, the corresponding Hamiltonian is proportional to either the Laplacian or the adjacency matrix of the graph. The two quantum walks are equivalent on regular graphs, since each vertex has the same degree. However, for irregular graphs, the evolutions of the two quantum walks are generally different. In this paper, we report an experimental investigation of the two quantum walks on irregular graphs with single photons and interferometric networks. We demonstrate that it is possible to obtain equivalent probability distributions with the two quantum walks on specific irregular graphs, where the particle is initially localized at a vertex or uniformly distributed at multiple vertices. Our results not only deepen the understanding of the equivalence between the two quantum walks, but also extend the application of the continuous-time quantum walk.

DOI: 10.1103/PhysRevA.105.062448

I. INTRODUCTION

The main pursuit of quantum information is to design large-scale general-purpose quantum computers [1,2]. An effective platform to develop quantum algorithms is the quantum walk (QW) [3], which is the quantum analog of a classical random walk. In QW, a walker can be in superposition of multiple states so that it propagates in superposition of possible paths. Therefore, QW spreads quadratically faster through the interference between paths and entanglement between different degrees of freedom [4,5]. It is useful for a wide range of applications including search algorithms [6–10], quantum simulation [11–13], and universal quantum computation [14–16].

Similar to a classical random walk, QW has two forms [17]: the discrete-time quantum walk, which uses a quantum coin to govern the direction of walk; and the continuous-time quantum walk (CTQW) [18], which directly defines the walk in discrete position space through a time-varying unitary matrix that depends on the Hamiltonian of the physical system. Traditionally, for the CTQW, the space is represented by a graph, which gives its discrete Laplacian as the Hamiltonian [7,18–22]. Another kind of Hamiltonian is provided by the adjacency matrix [9,23–28].

The Laplacian is usually used for discrete approximation to the kinetic energy operator of quantum mechanics [29–36], and the adjacency matrix is used for quantum computation [8,14,37–41]. We refer to the two QWs as the Laplacian QW and the adjacency QW. The distinction between the Laplacian QW and the adjacency QW has been explored in terms of search algorithms [42] and perfect state transfer [20,43].

For the CTQW on a regular graph, where vertices have the same number of neighbors, the evolutions of the two QWs are equivalent [27,30,44–46]. Thus, the probability distributions of particles are identical in position space. From a conceptual point of view, an irregular graph has vertices with different degrees, so the probability distributions of the two QWs generally show differences. However, Wong and Lockhart have shown that the probability distributions of the two QWs are identical on some specific irregular graphs when the walker starts from a certain vertex [46]. The equivalence of the two CTQWs has the potential to realize some practical applications. For specific physical systems, the way to experimentally realize two models of QWs might be different. That is, the resources or complexity required to realize the Laplacian and adjacency QWs might be different. In that case, we can choose the model at low cost or low complexity to achieve the application as the two models are proven to be equal for some certain applications.

In this paper, we report an experimental simulation of the Laplacian and the adjacency QWs on irregular graphs with single photons and interferometric networks. Our results demonstrate the equivalence of two QWs on five-vertex and six-vertex irregular graphs with the walker initially localized at a certain vertex, which support the prediction in Ref. [46]. In addition, we confirm that such equivalence depends on the

*dkqu@seu.edu.cn
†gnep.eux@gmail.com

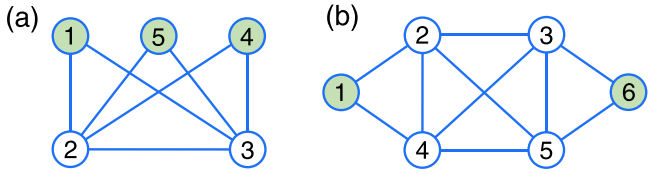

FIG. 1. (a) Irregular graphs with (a) five and (b) six vertices. The probability distributions of the two QWs are equivalent, if the particle is initially localized at one of the green vertices.

initial state. Interestingly, we show that equivalence can also exist even when the walker is initially distributed at multiple vertices.

This paper is organized as follows. In Sec. II, we give a brief introduction to the CTQW and illustrate it with irregular graphs. In Sec. III, we experimentally demonstrate the Laplacian QW and the adjacency QW on the five-vertex irregular graph and the six-vertex irregular graph. Section IV contains the experimental results of the equivalence of the two QWs. We conclude with a summary of our observations in Sec. V.

II. CTQWs ON IRREGULAR GRAPHS

The CTQW is the evolution of a particle in discrete space governed by Schrödinger's equation

$$i\frac{d}{dt}|\psi\rangle = H|\psi\rangle, \tag{1}$$

where we set $\hbar = 1$. The state of the walker at time t is $|\psi(t)\rangle = e^{-iHt}|\psi(0)\rangle$ and the probability that it is localized at vertex x is $P(x,t) = |\langle x|\psi(t)\rangle|^2$, where $\{|x\rangle\}$ constitutes the orthonormal basis spanning the space of the vertices.

As shown in Fig. 1, the discrete space can be represented by a graph $G(V,E)$ composed of vertices $i \in V$ and edges $(i,j) \in E$. The adjacency matrix A of a graph is defined as

$$A_{ij} = \begin{cases} 1, & (i,j) \in E, \\ 0, & (i,j) \notin E. \end{cases} \tag{2}$$

For a free particle, the Hamiltonian is the kinetic energy of the particle $H = -\gamma L$, which is proportional to the negative of the Laplacian $L = A - D$. Here, γ is the jumping rate of the walk and D is the diagonal matrix, where the diagonal entries $D_{ii} = \deg(i)$ represent the degree of vertex i. In some applications, e.g., search algorithms [9] and PageRank [28,47], the corresponding Hamiltonian is instead proportional to the negative of the adjacency matrix A, $H = -\gamma A$. In this paper, we choose $\gamma = 1$.

For a regular graph, each vertex has the same degree d, so $D = dI$, where I is the identity matrix. In this case, the state of the Laplacian QW $|\psi_L(t)\rangle$ differs from that of the adjacency QW $|\psi_A(t)\rangle$ by a global phase, $|\psi_L(t)\rangle = e^{iLt}|\psi(0)\rangle = e^{-idt}|\psi_A(t)\rangle$. Therefore, the probability distributions of the two QWs are equivalent, $P_L(x,t) = |\langle x|\psi_L(t)\rangle|^2 = |\langle x|\psi_A(t)\rangle|^2 = P_A(x,t)$.

For an irregular graph, some vertices have different degrees, and the probability distributions of the two QWs are generally different. However, for some specific irregular graphs and localized initial states, equivalence can still be obtained. Wong and Lockhart [46] present eight families of irregular graphs and analytically prove that the two QWs on these graphs are equivalent when starting at a certain vertex.

In this paper, we consider two examples of irregular graphs proposed by Wong and Lockhart [46]. One is an irregular graph with five vertices as shown in Fig. 1. Its adjacency matrix A and the Laplacian L are

$$A = \begin{pmatrix} 0 & 1 & 1 & 0 & 0 \\ 1 & 0 & 1 & 1 & 1 \\ 1 & 1 & 0 & 1 & 1 \\ 0 & 1 & 1 & 0 & 0 \\ 0 & 1 & 1 & 0 & 0 \end{pmatrix},$$

$$L = \begin{pmatrix} -2 & 1 & 1 & 0 & 0 \\ 1 & -4 & 1 & 1 & 1 \\ 1 & 1 & -4 & 1 & 1 \\ 0 & 1 & 1 & -2 & 0 \\ 0 & 1 & 1 & 0 & -2 \end{pmatrix},$$

respectively. For this graph, the two QWs will have the same probability distribution when the initial state is localized at one of the green vertices, as shown in Fig. 1(a). Moreover, when the initial state is a uniform superposition over vertices 2 and 3, and vertices 1, 4, and 5, the probability distributions of the two QW are also identical. In Sec. III, we elaborate on the formula for the superposition states.

The other irregular graph has six vertices as shown in Fig. 1(b), which has the adjacency matrix A' and the Laplacian L' as

$$A' = \begin{pmatrix} 0 & 1 & 0 & 1 & 0 & 0 \\ 1 & 0 & 1 & 1 & 1 & 0 \\ 0 & 1 & 0 & 1 & 1 & 1 \\ 1 & 1 & 1 & 0 & 1 & 0 \\ 0 & 1 & 1 & 1 & 0 & 1 \\ 0 & 0 & 1 & 0 & 1 & 0 \end{pmatrix},$$

$$L' = \begin{pmatrix} -2 & 1 & 0 & 1 & 0 & 0 \\ 1 & -4 & 1 & 1 & 1 & 0 \\ 0 & 1 & -4 & 1 & 1 & 1 \\ 1 & 1 & 1 & -4 & 1 & 0 \\ 0 & 1 & 1 & 1 & -4 & 1 \\ 0 & 0 & 1 & 0 & 1 & -2 \end{pmatrix},$$

respectively. For the irregular graph with six vertices, the two QWs have the same probability distribution, where the walker is initially localized at one of the green vertices 1 and 6. Moreover, the equivalence of the probability distributions of the two QWs is also satisfied for the initial state with equal weights at vertices 2 and 4 or equal weights at vertices 3 and 5.

III. EXPERIMENT DEMONSTRATION

We first demonstrate the experimental test of the identical probability distributions of the two QWs on the irregular graph with five vertices. As shown in Fig. 2(a), the experimental setup consists of three stages: the initial-state preparation, the time evolution of the Laplacian or adjacency QW, and project measurements. The basis states of the five-dimensional qudit are encoded as $\{|1\rangle = |V_1\rangle, |2\rangle = |H_2\rangle, |3\rangle = |V_2\rangle, |4\rangle = |H_3\rangle, |5\rangle = |V_3\rangle\}$, where H (V)

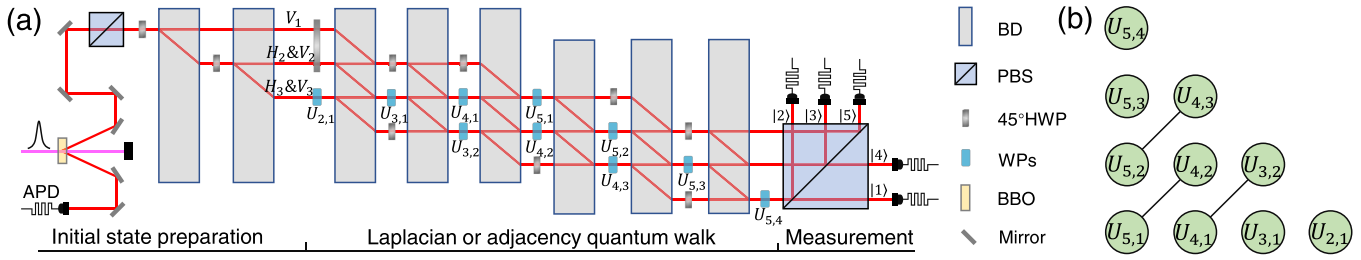

FIG. 2. (a) Experimental setup. The heralded single photons are generated and are injected into the optical network to simulate the CTQW on irregular graphs. The first polarizing beam splitter (PBS), half-wave plates (HWPs), and two beam displacers (BDs) are used to prepare the initial states. The Laplacian and adjacency QWs can be simulated by an interferometric network, consisting of WPs and BDs. The probability distributions are obtained by projecting the final state into the basis states via a PBS. The photons are detected by APDs. (b) The 5×5 unitary matrix is decomposed into a product of ten two-level unitary matrices. The green nodes represent the two-level unitary operators. The connection between two matrices indicates that they can be realized at the same time.

denotes the horizontal (vertical) polarizations with the subscript k ($k = 1, 2, 3$) denoting the spatial mode.

In the preparation stage, a pair of photons are generated via spontaneous parametric down-conversion (SPDC) using a β-barium-borate (BBO) crystal. As one trigger photon is detected by a single-photon avalanche photodiode (APD), the signal photon is heralded and injected into the interferometric network. A polarization beam splitter (PBS), two beam displacers (BDs), and two half-wave plates (HWPs) are used to prepare the state of the photonic five-dimensional system in different initial states. In the experiment, we prepare four initial states, which are

$$|\psi(0)\rangle = \begin{cases} (1 \quad 0 \quad 0 \quad 0 \quad 0)^{\mathsf{T}}, & \text{vertex 1,} \\ (0 \quad 1 \quad 0 \quad 0 \quad 0)^{\mathsf{T}}, & \text{vertex 2,} \\ (0 \quad 1 \quad 1 \quad 0 \quad 0)^{\mathsf{T}}/\sqrt{2}, & \text{vertices 2 and 3,} \\ (1 \quad 0 \quad 0 \quad 1 \quad 1)^{\mathsf{T}}/\sqrt{3}, & \text{vertices 1, 4, and 5.} \end{cases} \tag{3}$$

In order to demonstrate the dynamics of CTQWs' e^{-iHt} conveniently and flexibly, the evolution time can be regard as a parameter of the unitary operation. Different time parameters correspond to different unitary matrices. To implement the unitary operations, we decompose the matrix into a product of ten two-level unitary matrices $U_{m,n}$ [9,48,49], where $m \in \{2, \ldots, 5\}$ and $n \in \{1, \ldots, 4\}$. Here, $U_{m,n}$ denotes the two-level unitary matrix that acts only on two vector components, m and n, in five-dimensional Hilbert space with the complementary vector components unchanged. For example, $U_{4,2}$ means that the two-level unitary matrix acts only on the fourth and second vector components in five-dimensional Hilbert space. The decomposition of a unitary operator is

$$U = U_{5,4} \cdots U_{5,1} U_{4,3} \cdots U_{4,1} \cdots U_{2,1}. \tag{4}$$

Through this decomposition, the two-level unitary matrices $U_{m,n}$ and $U_{m-1,n+1}$ can be implemented simultaneously in the interferometric networks, thus reducing the number of optical elements as shown in Fig. 2(b). To realize $U_{m,n}$, we first combine the corresponding spatial modes using a BD, and then realize the 2×2 unitary matrices using the array of wave plates (WPs). Therefore, in the experimental simulation, the difference between the unitary operators of the two QWs, U_L and U_A, lies in the parameters of the ten sets of WPs. We realize unitary operators $U_L = e^{iLt}$ and $U_A = e^{iAt}$ for $t = \{10, 10^2, 10^3, 10^4\}$ in the experiment. Experimentally, we can adjust the time parameters using the wave-plate angles.

In the measurement stage, the probability of the final state distributed at every vertex is obtained by a projective measurement. A PBS projects the final state into the basis states $|x\rangle$ ($x = 1, \ldots, 5$). The output photons are finally detected

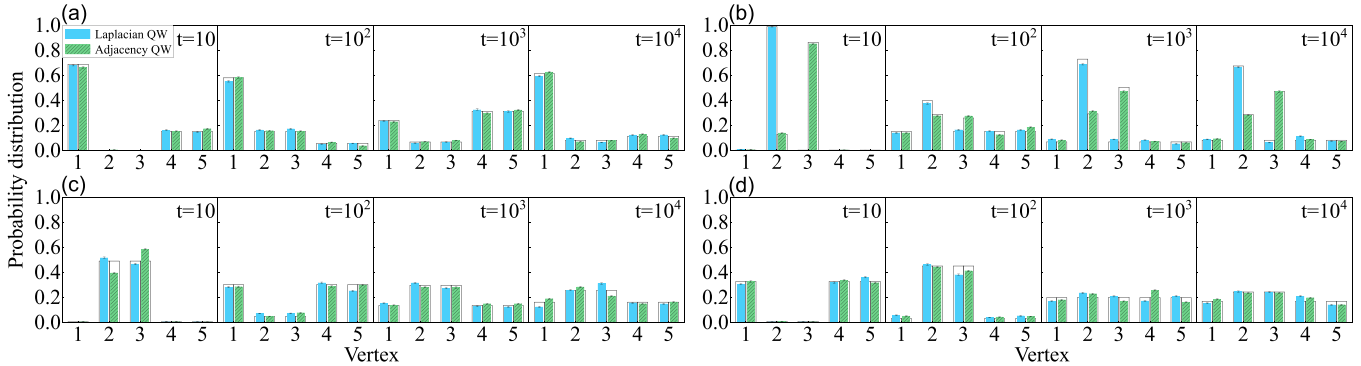

FIG. 3. Experimental results of the probability distributions of two QWs at time $t = \{10, 10^2, 10^3, 10^4\}$ for the irregular graph with five vertices. The blue and green hatched bars represent the experimental results of the Laplacian and adjacency QWs, respectively. The open bars correspond to the theoretical predictions of the probability distributions of the two QWs. (a)–(d) indicate the results for QW starting at vertex 1, vertex 2, vertices 2 and 3, and vertices 1, 4, and 5, respectively. Error bars indicate the statistical uncertainty, which are obtained based on assuming Poissonian statistics.

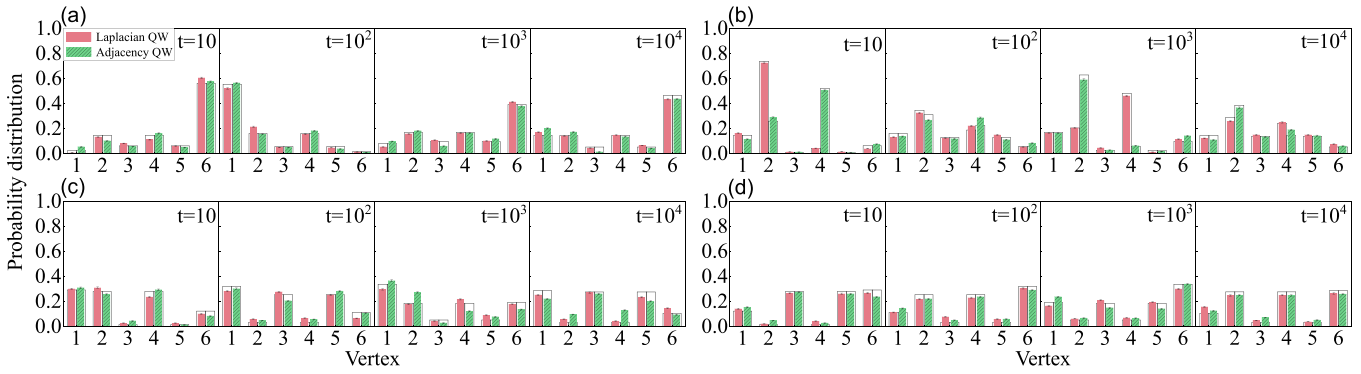

FIG. 4. Experimental results of the probability distributions of two QWs at time $t = \{10, 10^2, 10^3, 10^4\}$ for the irregular graph with six vertices. The red and green hatched bars represent the experimental results of the Laplacian and adjacency QWs, respectively. The open bars correspond to the theoretical predictions of the probability distributions of the two QWs. (a)–(d) indicate the results of the two QWs when starting at vertex 1, vertex 2, vertices 2 and 4, and vertices 3 and 5, respectively. Error bars indicate the statistical uncertainty, which is obtained based on assuming Poissonian statistics.

by APDs, in coincidence with the trigger photon. For each setup, we record clicks for 1 s and register about 8000 single photons. For the Laplacian (adjacency) QW at time t, we can obtain the number of photons at vertex x, $N_{L(A)}(x,t)$. Therefore, the probability of the final state localized at vertex x can be evaluated as $P_{L(A)}(x,t) = N_{L(A)}(x,t)/\sum_x N_{L(A)}(x,t)$.

For the irregular graph with six vertices, the experimental simulation is similar to that with five vertices. In this case, the basis states of the six-dimensional qudit are encoded as $\{|1\rangle = |H_1\rangle, |2\rangle = |V_1\rangle, |3\rangle = |H_2\rangle, |4\rangle = |V_2\rangle, |5\rangle = |H_3\rangle, |6\rangle = |V_3\rangle\}$. We prepare the initial states of the system as

$$|\psi(0)\rangle = \begin{cases} (1\ 0\ 0\ 0\ 0\ 0)^{\mathsf{T}}, & \text{vertex 1,} \\ (0\ 1\ 0\ 0\ 0\ 0)^{\mathsf{T}}, & \text{vertex 2,} \\ (0\ 1\ 0\ 1\ 0\ 0)^{\mathsf{T}}/\sqrt{2}, & \text{vertices 2 and 4,} \\ (0\ 0\ 1\ 0\ 1\ 0)^{\mathsf{T}}/\sqrt{2}, & \text{vertices 3 and 5.} \end{cases} \tag{5}$$

The six-dimensional evolution operator can be decomposed into a product of 15 two-level unitary matrices $U_{m',n'}$, where $m' \in \{2,\ldots,6\}$ and $n' \in \{1,\ldots,5\}$. We realize the 6×6 unitary operators by using 15 sets of WPs and a complex interferometric network. There are at most three two-level unitary matrices that can be realized simultaneously, i.e., $U_{6,1}$, $U_{5,2}$, and $U_{4,3}$. Through this approach, our experiment can also be generalized to simulations of CTQWs for graphs with more vertices [9].

IV. EXPERIMENT RESULTS

For each experiment, we evaluate the probability distributions of the two QWs. The experiment results for the five (six)-vertex graph are shown in Fig. 3 (Fig. 4).

For both graphs, the Laplacian and adjacency QWs have the same probability distribution when the initial state is localized in vertex 1 as shown in Figs. 3(a) and 4(a), which verifies the equivalence as predicted by Wong and Lockhart [46]. Moreover, the probability distributions are different when the initial state is localized at vertex 2, as shown in Figs. 3(b) and 4(b). Therefore, the equivalence of the probability distributions is state dependent.

We also measure the probability distributions where the initial state is in a uniform superposition over multiple vertices. In Figs. 3(c) and 3(d), our experimental results show that the two QWs on the irregular graph with five vertices evolve with the same probability distribution when the initial state is distributed in either the equal superposition of vertices 2 and 3, or that of vertices 1, 4, and 5. The probability distributions of the two QWs on the irregular graph with six vertices are still equal when the initial state is distributed in the equal superposition of vertices 2 and 4, or that of vertices 3 and 5 as shown in Figs. 4(c) and 4(d).

To quantify the equivalence between the probability distributions of the two QWs, we calculate the similarity between the measured probability distributions of the two QWs at time t [12,50–53],

$$S(t) = \left(\sum_x \sqrt{P_L(x,t)P_A(x,t)}\right)^2. \tag{6}$$

The similarity varies between 0 for completely different distributions and 1 for identical distributions. The results of the similarities are presented in Table I. For the

TABLE I. The similarities between the measured probability distributions of the Laplacian and adjacency QWs.

	Irregular graph with five vertices			
	$t = 10$	$t = 10^2$	$t = 10^3$	$t = 10^4$
From 1	0.9976(8)	0.9959(10)	0.9977(7)	0.9950(11)
From 2	0.1612(58)	0.9768(23)	0.7877(63)	0.7454(69)
From 2 and 3	0.9836(20)	0.9949(11)	0.9968(9)	0.9824(21)
From 1, 4, and 5	0.9975(8)	0.9988(5)	0.9859(19)	0.9982(6)
	Irregular graph with six vertices			
	$t = 10$	$t = 10^2$	$t = 10^3$	$t = 10^4$
From 1	0.9684(27)	0.9923(13)	0.9853(19)	0.9860(18)
From 2	0.6664(73)	0.9866(18)	0.7346(70)	0.9848(19)
From 2 and 4	0.9885(17)	0.9875(17)	0.9677(28)	0.9649(29)
From 3 and 5	0.9916(14)	0.9946(12)	0.9830(20)	0.9949(11)

irregular graph with five vertices, we get the minimum similarity of the two QWs when starting at vertices 2 and 3, $S(10^4) = 0.9824 \pm 0.0021$. For the irregular graph with six vertices, the minimum similarity of probability distributions of the two QWs measured in the experiment when starting at vertices 2 and 4 is $S(10^4) = 0.9649 \pm 0.0029$. The reason for the larger uncertainty is that the experimental implementation of the 6×6 unitary matrix requires more complex interferometric networks.

The experimental results agree with the theoretical prediction very well. The imperfection of the experiment is mainly caused by the accuracy of the WPs and the dephasing introduced via the misalignment of the BDs, two of which form a Mach-Zehnder interferometer. Thus, we experimentally demonstrate that on irregular graphs, there is equivalence between Laplacian and adjacency QWs, which depends on both the graphs and the initial states.

V. DISCUSSION AND CONCLUSIONS

In summary, we have investigated the probability distributions of the Laplacian and adjacency QWs on irregular graphs with five and six vertices using single photons and interferometric networks. We can decompose an arbitrary $n \times n$ unitary matrix into $n(n-1)/2$ two-level unitary matrices. Our experimental setup directly implements the two-level unitary matrices in a bulk optical system, the advantage of which is the flexibility to demonstrate the dynamics of CTQWs [9]. The experimental results agree with the prediction proposed by Wong *et al.* [46], i.e., they have the same probability distribution over the vertices when the walker is initially at a certain vertex. Our experiments also show that this equivalence depends on the initial state. However, we find and experimentally show that the equivalence between the probability distributions of the two QWs can also be observed even when the walker starts from an equal superposition of specific multiple vertices.

The significance of our experiments is the experimental verification and demonstration of the existence of this equivalence. For large-scale irregular graphs, the number of spatial modes N_s and the number of bulk optical elements (BDs) N_{BD} increase with the number of vertices n, i.e., $N_s \sim \lceil n/2 \rceil$ and $N_{\mathrm{BD}} \sim 2n - 4$. Moreover, our method can be applied to the recently developed waveguide technology, which promises breakthroughs in stability and scalability.

The Laplacian and adjacency QWs are preferred for certain applications. The choice of the Laplacian and the adjacency matrix affects the efficiency of quantum search algorithms [42]. In the case of searching on such an irregular graph, there may be equivalence in the search efficiencies of the two QWs. Furthermore, there are some potential applications of our work, i.e., the equivalence of the two QWs on irregular graphs. For specific physical systems, the way to experimentally realize two models of QWs might be different. That is, the resources or complexity required to realize the Laplacian and adjacency QWs might be different. In that case, we can choose the model at low cost or low complexity to achieve the application as the two models are proven to be equal for some certain applications. There is still a great deal we need to learn about the Laplacian and the adjacency matrix. For the two QWs, the evolution on more complex irregular graphs is a possible area of research. Whether there are more initial states can still satisfy the equivalence of the two QWs. Our work deepens the understanding of the Laplacian and the adjacency matrix and sheds light on accelerating the development of quantum computation.

ACKNOWLEDGMENTS

This work has been supported by the National Natural Science Foundation of China (Grants No. 12025401, No. U1930402, No. 12004184, No. 12104036, No. 12104009, and No. 12088101). X.Z. is supported by the Natural Science Foundation of Jiangsu Province (Grant No. BK20190428).

[1] A. Montanaro, Quantum algorithms: An overview, npj Quantum Inf. **2**, 15023 (2016).
[2] A. W. Harrow and A. Montanaro, Quantum computational supremacy, Nature (London) **549**, 203 (2017).
[3] Y. Aharonov, L. Davidovich, and N. Zagury, Quantum random walks, Phys. Rev. A **48**, 1687 (1993).
[4] S. Dadras, A. Gresch, C. Groiseau, S. Wimberger, and G. S. Summy, Quantum Walk in Momentum Space with a Bose-Einstein Condensate, Phys. Rev. Lett. **121**, 070402 (2018).
[5] P. Xue, B. C. Sanders, and D. Leibfried, Quantum Walk on a Line for a Trapped Ion, Phys. Rev. Lett. **103**, 183602 (2009).
[6] N. Shenvi, J. Kempe, and K. B. Whaley, Quantum random-walk search algorithm, Phys. Rev. A **67**, 052307 (2003).
[7] A. M. Childs and J. Goldstone, Spatial search by quantum walk, Phys. Rev. A **70**, 022314 (2004).
[8] S. Chakraborty, L. Novo, A. Ambainis, and Y. Omar, Spatial Search by Quantum Walk is Optimal for Almost all Graphs, Phys. Rev. Lett. **116**, 100501 (2016).
[9] D. Qu, S. Marsh, K. Wang, L. Xiao, J. Wang, and P. Xue, Deterministic Search on Star Graphs via Quantum Walks, Phys. Rev. Lett. **128**, 050501 (2022).
[10] N. Pan, T. Chen, H. Sun, and X. Zhang, Electric-circuit realization of fast quantum search, Research **2021**, 9793071 (2021).
[11] L. Xiao, X. Zhan, Z. H. Bian, K. K. Wang, X. Zhang, X. P. Wang, J. Li, K. Mochizuki, D. Kim, N. Kawakami, W. Yi, H. Obuse, B. C. Sanders, and P. Xue, Observation of topological edge states in parity–time-symmetric quantum walks, Nat. Phys. **13**, 1117 (2017).
[12] X. Zhan, L. Xiao, Z. Bian, K. Wang, X. Qiu, B. C. Sanders, W. Yi, and P. Xue, Detecting Topological Invariants in Nonunitary Discrete-Time Quantum Walks, Phys. Rev. Lett. **119**, 130501 (2017).
[13] K. Wang, X. Qiu, L. Xiao, X. Zhan, Z. Bian, W. Yi, and P. Xue, Simulating Dynamic Quantum Phase Transitions in Photonic Quantum Walks, Phys. Rev. Lett. **122**, 020501 (2019).

[14] A. M. Childs, Universal Computation by Quantum Walk, Phys. Rev. Lett. **102**, 180501 (2009).

[15] N. B. Lovett, S. Cooper, M. Everitt, M. Trevers, and V. Kendon, Universal quantum computation using the discrete-time quantum walk, Phys. Rev. A **81**, 042330 (2010).

[16] A. M. Childs, D. Gosset, and Z. Webb, Universal computation by multiparticle quantum walk, Science **339**, 791 (2013).

[17] F. W. Strauch, Connecting the discrete- and continuous-time quantum walks, Phys. Rev. A **74**, 030301(R) (2006).

[18] E. Farhi and S. Gutmann, Quantum computation and decision trees, Phys. Rev. A **58**, 915 (1998).

[19] E. Agliari, A. Blumen, and O. Mülken, Quantum-walk approach to searching on fractal structures, Phys. Rev. A **82**, 012305 (2010).

[20] R. Alvir, S. Dever, B. Lovitz, J. Myer, C. Tamon, Y. Xu, and H. Zhan, Perfect state transfer in Laplacian quantum walk, J. Algebr. Comb. **43**, 801 (2016).

[21] P. Chawla, C. V. Ambarish, and C. M. Chandrashekar, Quantum percolation in quasicrystals using continuous-time quantum walk, J. Phys. Commun. **3**, 125004 (2019).

[22] T. Wu, J. A. Izaac, Z.-X. Li, K. Wang, Z.-Z. Chen, S. Zhu, J. B. Wang, and X.-S. Ma, Experimental Parity-Time Symmetric Quantum Walks for Centrality Ranking on Directed Graphs, Phys. Rev. Lett. **125**, 240501 (2020).

[23] E. Farhi, J. Goldstone, and S. Gutmann, A quantum algorithm for the Hamiltonian NAND tree, Theory Comput. **4**, 169 (2008).

[24] S. Bose, A. Casaccino, S. Mancini, and S. Severini, Communication in XYZ all-to-all quantum networks with a missing link, Int. J. Quantum Inf. **07**, 713 (2009).

[25] C. Godsil, State transfer on graphs, Discrete Math. **312**, 129 (2012).

[26] L. Novo, S. Chakraborty, M. Mohseni, H. Neven, and Y. Omar, Systematic dimensionality reduction for quantum walks: Optimal spatial search and transport on non-regular graphs, Sci. Rep. **5**, 13304 (2015).

[27] J. A. Izaac, X. Zhan, Z. Bian, K. Wang, J. Li, J. B. Wang, and P. Xue, Centrality measure based on continuous-time quantum walks and experimental realization, Phys. Rev. A **95**, 032318 (2017).

[28] K. Wang, Y. Shi, L. Xiao, J. Wang, Y. N. Joglekar, and P. Xue, Experimental realization of continuous-time quantum walks on directed graphs and their application in PageRank, Optica **7**, 1524 (2020).

[29] R. Guantes and S. C. Farantos, High order finite difference algorithms for solving the Schrödinger equation in molecular dynamics, J. Chem. Phys. **111**, 10827 (1999).

[30] P. Kurzyński and A. Wójcik, Discrete-time quantum walk approach to state transfer, Phys. Rev. A **83**, 062315 (2011).

[31] T. G. Wong and P. Philipp, Engineering the success of quantum walk search using weighted graphs, Phys. Rev. A **94**, 022304 (2016).

[32] J. A. Izaac and J. B. Wang, Systematic dimensionality reduction for continuous-time quantum walks of interacting fermions, Phys. Rev. E **96**, 032136 (2017).

[33] R. Babbush, N. Wiebe, J. McClean, J. McClain, H. Neven, and G. K.-L. Chan, Low-Depth Quantum Simulation of Materials, Phys. Rev. X **8**, 011044 (2018).

[34] L. Razzoli, M. G. A. Paris, and P. Bordone, Continuous-time quantum walks on planar lattices and the role of the magnetic field, Phys. Rev. A **101**, 032336 (2020).

[35] J. R. McClean, M. P. Harrigan, M. Mohseni, N. C. Rubin, Z. Jiang, S. Boixo, V. N. Smelyanskiy, R. Babbush, and H. Neven, Low-depth mechanisms for quantum optimization, PRX Quantum **2**, 030312 (2021).

[36] A. Candeloro, L. Razzoli, P. Bordone, and M. G. A. Paris, Role of topology in determining the precision of a finite thermometer, Phys. Rev. E **104**, 014136 (2021).

[37] M. Santha, Quantum walk based search algorithms, in *Theory and Applications of Models of Computation* (Springer, Berlin, 2008), pp. 31–46

[38] D. Gosset, B. M. Terhal, and A. Vershynina, Universal Adiabatic Quantum Computation via the Space-Time Circuit-to-Hamiltonian Construction, Phys. Rev. Lett. **114**, 140501 (2015).

[39] X. Qiang, T. Loke, A. Montanaro, K. Aungskunsiri, X. Zhou, J. L. O'Brien, J. B. Wang, and J. C. F. Matthews, Efficient quantum walk on a quantum processor, Nat. Commun. **7**, 11511 (2016).

[40] T. Osada, B. Coutinho, Y. Omar, K. Sanaka, W. J. Munro, and K. Nemoto, Continuous-time quantum-walk spatial search on the Bollobás scale-free network, Phys. Rev. A **101**, 022310 (2020).

[41] X. Qiang, Y. Wang, S. Xue, R. Ge, L. Chen, Y. Liu, A. Huang, X. Fu, P. Xu, T. Yi, F. Xu, M. Deng, J. B. Wang, J. D. A. Meinecke, J. C. F. Matthews, X. Cai, X. Yang, and J. Wu, Implementing graph-theoretic quantum algorithms on a silicon photonic quantum walk processor, Sci. Adv. **7**, eabb8375 (2021).

[42] T. G. Wong, L. Tarrataca, and N. Nahimov, Laplacian versus adjacency matrix in quantum walk search, Quantum Inf. Process. **15**, 4029 (2016).

[43] M. Christandl, N. Datta, A. Ekert, and A. J. Landahl, Perfect State Transfer in Quantum Spin Networks, Phys. Rev. Lett. **92**, 187902 (2004).

[44] Y. Elon, Eigenvectors of the discrete Laplacian on regular graphs—a statistical approach, J. Phys. A: Math. Theor. **41**, 435203 (2008).

[45] A. Abiad, B. Brimkov, A. Erey, L. Leshock, X. Martínez-Rivera, S. O, S.-Y. Song, and J. Williford, On the Wiener index, distance cospectrality and transmission-regular graphs, Discrete Appl. Math. **230**, 1 (2017).

[46] T. G. Wong and J. Lockhart, Equivalent Laplacian and adjacency quantum walks on irregular graphs, Phys. Rev. A **104**, 042221 (2021).

[47] Y. Wang, S. Xue, J. Wu, and P. Xu, Continuous-time quantum walk based centrality testing on weighted graphs, Sci. Rep. **12**, 6001 (2022).

[48] M. A. Nielsen and I. L. Chuang, *Quantum Computation and Quantum Information: 10th Anniversary Edition* (Cambridge University Press, Cambridge, UK, 2010).

[49] K. Wang, G. C. Knee, X. Zhan, Z. Bian, J. Li, and P. Xue, Optimal experimental demonstration of error-tolerant quantum witnesses, Phys. Rev. A **95**, 032122 (2017).

[50] A. Schreiber, A. Gábris, P. P. Rohde, K. Laiho, M. Štefaňák, V. Potoček, C. Hamilton, I. Jex, and C. Silberhorn, A 2D quantum walk simulation of two-particle dynamics, Science **336**, 55 (2012).

[51] A. Crespi, R. Osellame, R. Ramponi, V. Giovannetti, R. Fazio, L. Sansoni, F. De Nicola, F. Sciarrino, and P. Mataloni,

Anderson localization of entangled photons in an integrated quantum walk, Nat. Photonics **7**, 322 (2013).

[52] B. Wang, T. Chen, and X. Zhang, Experimental Observation of Topologically Protected Bound States with Vanishing Chern Numbers in a Two-Dimensional Quantum Walk, Phys. Rev. Lett. **121**, 100501 (2018).

[53] Y. F. Peng, W. Wang, and X. X. Yi, Discrete-time quantum walk with time-correlated noise, Phys. Rev. A **103**, 032205 (2021).